J Biomol NMR (2010) 47:171–181
DOI 10.1007/s10858-010-9421-0

ARTICLE

HA-detected experiments for the backbone assignment of intrinsically disordered proteins

Sampo Mäntylahti · Olli Aitio · Maarit Hellman · Perttu Permi

Received: 2 February 2010 / Accepted: 12 April 2010 / Published online: 1 May 2010

Abstract We propose a new alpha proton detection based approach for the sequential assignment of natively unfolded proteins. The proposed protocol superimposes on following features: HA-detection (1) enables assignment of natively unfolded proteins at any pH, i.e., it is not sensitive to rapid chemical exchange undergoing in natively unfolded proteins even at moderately high pH. (2) It allows straightforward assignment of proline-rich polypeptides without additional proline-customized experiments. (3) It offers more streamlined and less ambiguous assignment based on solely intraresidual $^{15}N(i)$-$^{13}C'(i)$-$H^{\alpha}(i)$ (or $^{15}N(i)$-$^{13}C^{\alpha}(i)$-$H^{\alpha}(i)$) and sequential $^{15}N(i+1)$-$^{13}C'(i)$-$H^{\alpha}(i)$ (or $^{15}N(i+1)$-$^{13}C^{\alpha}(i)$-$H^{\alpha}(i)$) correlation experiments together with efficient use of chemical shifts of ^{15}N and $^{13}C'$ nuclei, which show smaller dependence on residue type. We have tested the proposed protocol on two proteins, small globular 56-residue GB1, and highly disordered, proline-rich 47-residue fifth repeat of $EspF_U$. Using the proposed approach, we were able to assign 90% of $^{1}H^{\alpha}$, $^{13}C^{\alpha}$, $^{13}C'$, ^{15}N chemical shifts in $EspF_U$. We reckon that the HA-detection based strategy will be very useful in the assignment of natively unfolded proline-rich proteins or polypeptide chains.

Keywords Assignment · $EspF_U$ · H(CA)CON · iH(CA)NCO · Intrinsically unfolded proteins

Electronic supplementary material The online version of this article (doi:10.1007/s10858-010-9421-0) contains supplementary material, which is available to authorized users.

S. Mäntylahti · O. Aitio · M. Hellman · P. Permi (✉)
Program in Structural Biology and Biophysics, Institute of Biotechnology/NMR Laboratory, University of Helsinki, P.O. Box 65, 00014 Helsinki, Finland
e-mail: Perttu.Permi@helsinki.fi

Introduction

NMR spectroscopy has become an invaluable biophysical tool for characterization of variety of biological macromolecules in solution. During the past 20 years bewildering myriad of triple-resonance experiments have been developed for the assignment of protein backbone and sidechain nuclei (for review, see e.g., Sattler et al. 1999; Permi and Annila 2004). Studies of larger proteins usually utilizes (per)deuteration (Yamazaki et al. 1994) and so-called TROSY effect (Pervushin et al. 1997). These innovations have rendered pulse sequences based on alpha proton (HA) detection inferior compared to experiments which detect amide proton (HN) during acquistion. However, HN-detection is not always an optimal choice for assignment. Intrinsically unfolded proteins (IUPs) are a particular class of biomolecules, which play pivotal role in signal transduction and various regulatory processes (Tompa 2002; Dyson and Wright 2005). Characterization IUPs utilizing HN-detection based approach may not yield satisfactory results. A major hurdle in studies of IUPs stems from the lack of diversity in proton chemical shifts due to highly similar chemical environment in polypeptides without well-defined three-dimensional structure. Lack of strict 3D structure of UIPs causes the chemical shift dispersion of protons to be highly degenerated, which results in multidimensional spectra exhibiting heavily overlapping cross peaks, which in turn makes the assignment of main-chain resonances particularly challenging. This becomes especially pronounced in the case of even modestly alkali (pH $\geq$ 7) conditions, where a rapid chemical exchange of exposed labile protons with water results in broad lines and, hence, in a decreased sensitivity and resolution for backbone amide protons (Bai et al. 1993; Grzesiek et al. 1997; Hu et al. 2007). In addition, proline is one of the

most abundant residues in IUPs (Tompa 2002), and these proteins often contain multiple polyproline stretches, which render the sequential assignment strategy based on HN-detected triple-resonance experiments less useful.

Nearly unrestricted motional freedom makes the relaxation properties of IUPs ideal for multidimensional NMR studies, enabling development and application of sophisticated pulse sequences for their analysis. Our group has been developing and successfully applying HN-detected intraresidual experiments for the assignment of highly disordered proteins (Alho et al. 2007; Mäntylahti et al. 2009).

It is possible to employ pulse sequences that utilize highly selective coherence transfer pathways and provide non-redundant information with minimal spectral overlap without sacrificing too much in sensitivity. In case of IUPs, selective intraresidual and sequential HA-detected triple-resonance experiments can be put into a good use. In this paper we introduce novel HA-detected triple-resonance experiments, which correlate $^{1}H^{\alpha}$ chemical shift either with residues own $^{13}C(i)$ and $^{15}N(i)$ frequencies or the corresponding $^{15}N(i+1)$ frequency of the subsequent residue. The proposed experiments are complementary to the earlier developed proline optimized CDCA(NCO)CAHA (Bottomley et al. 1999) and HCAN/(HB)CBCA(CO)N(CA)HA (Kanelis et al. 2000) as well as recently introduced ^{13}C-detected experiments (Bermel et al. 2006, 2009). We have successfully employed this assignment strategy to a natively unfolded 47-residue fifth repeat of $EspF_u$ ($R47_5$) having a high content of proline residues and consecutive proline pairs (Cheng et al. 2008).

Results and discussion

Description of the pulse sequences

The schematic presentation of magnetization transfer route, and the proposed intraresidual iH(CA)NCO and iHCAN experiments for establishing correlations between $^{1}H^{\alpha}(i)$ $^{13}C'(i)$ and $^{15}N(i)$, and $^{1}H^{\alpha}(i)$, $^{13}C^{\alpha}(i)$ and $^{15}N(i)$ spins are shown in Fig. 1a–c, respectively. The corresponding schematics together with the sequential H(CA)CON pulse sequence for correlating $^{1}H_i^{\alpha}$ $^{13}C_i'$ and $^{15}N_{i+1}$ frequencies are shown in Fig. 1d, e. Inset in Fig. 1e′ displays an alternative implementation used for the $^{13}C'$ chemical shift labeling in the H(CA)CON experiment.

The flow of coherence during the intraresidual iH(CA)NCO and iHCAN experiments (Fig. 1b, c) can be described in the following way:

Fig. 1 **a** Schematic presentation of magnetization transfer pathway during the intraresidual experiments. *Bidirectional arrows* indicate out-and-back type magnetization transfer, whereas *one-way arrows* represent coherence transfer route which is unidirectional. *One-letter codes* above the *arrows* indicate time points in the pulse sequence. **b** Intraresidual iH(CA)NCO experiment to correlate $^{1}H^{\alpha}(i)$, $^{13}C'(i)$ and $^{15}N(i)$ chemical shifts and **c** intraresidual iHCAN experiment for correlating $^{1}H^{\alpha}(i)$, $^{13}C^{\alpha}(i)$ and $^{15}N(i)$ chemical shifts in uniformly ^{15}N, ^{13}C enriched proteins. **d** Schematic presentation of relay of coherence during the **e** H(CA)CON experiment, which correlates chemical shifts of $^{1}H^{\alpha}(i)$, $^{13}C'(i)$ and $^{15}N(i+1)$ resonances. **e′** Alternative implementation for the $^{13}C'$ chemical shift labeling during t_2. Narrow and wide rectangulars correspond to 90° and 180° flip angles, respectively, applied with phase x unless otherwise stated. The ^{1}H, ^{15}N, $^{13}C'$, and $^{13}C^{\alpha}$ carrier positions are 4.7 (water), 118 (center of ^{15}N spectral region), 175 ppm (center of $^{13}C'$ spectral region), and 57 ppm (center of $^{13}C^{\alpha}$ spectral region). The ^{13}C carrier is set initially to the middle of $^{13}C^{\alpha}$ region (57 ppm), shifted to 175 ppm just after the first 90° ^{13}C pulse (time point *a*), and shifted back to 57 ppm prior to time point *d*. All rectangular 90° pulses for $^{13}C^{\alpha}$ (57 ppm) and 180° pulses for $^{13}C'$ (175 ppm) were applied with durations of 40.4 μs (90°) and 36.2 μs (180°) at 800 MHz, respectively, in order to provide null mutual excitation (Kay et al. 1990). The first 180° pulse for $^{13}C^{\alpha}$ is an adiabatic, band-selective $^{13}C^{\alpha}$ inversion pulse with a sech/tanh profile and duration of 1 ms (Silver et al. 1984; Bendall 1995). The cascade of rectangular pulses on $^{13}C^{\alpha}$ denotes a composite pulse for ultra-broadband inversion with durations defined by $pwC^{*}(\beta_i/90)$, where β_i is a flip angle for individual pulses in the cascade i.e., 158.0, 171.2, 342.8, 145.5, 81.2, 85.3 (Shaka 1985). Two selective 90° pulses for $^{13}C'$ have the shape of center lobe of a sinc function and duration of 66.8 μs at 800 MHz. Phase modulated 180° pulses, applied off-resonance for $^{13}C^{\alpha}$, have the shape of one-lobe sinc profile and duration of 60.4 μs. The waltz-16 sequence (Shaka et al. 1983) with a strength of 4.8 kHz is employed to decouple ^{1}H spins during $2(T_{C'} + T_A + T_{CC}) - \tau_2$, t_1, and $2(T_N - \tau)$ periods. The adiabatic WURST field (Kupće and Wagner 1995) was used to decouple ^{13}C during acquisition. Delay durations: $\tau = 1/(4J_{HC})$ ~1.7 ms; $\tau_2 = 3.4$ ms (optimized for non-glycine residues) or 2.2–2.5 ms (for observing both glycine and non-glycine residues); ε = duration of G_H + field recovery ~0.4 ms; $T_C = 1/(2J_{C\alpha_{C'}})$ ~9.5 ms; $T_B = 1/(6J_{C\alpha_{C'}})$ ~3.3 ms; $T_A = 1/(4J_{C'N})$ ~16.6 ms; $T'_C = T_C + T_{CC}$; $T_{CC} = 1/(J_{C\alpha_{C\beta}}) - 1/(4J_{C'N}) - 1/(2J_{C\alpha_{C'}})$ ~0–2.5 ms; T_N ~14 ms; $t_{2,max} < 2.0{*}T'_C$. Frequency discrimination in ^{15}N and $^{13}C'$ dimensions is obtained using the States-TPPI protocol (Marion et al. 1989) applied to ϕ_1 and ϕ_2, respectively, whereas the quadrature detection in $^{13}C^{\alpha}$ dimension (scheme c) is obtained using the sensitivity-enhanced gradient selection (Kay et al. 1992; Schleucher et al. 1994). The echo and antiecho signals in $^{13}C^{\alpha}$ dimension are collected separately by inverting the sign of the G_C gradient pulse together with the inversion of ψ, respectively. Phase cycling: ϕ_1 = x, −x; ϕ_2 = 2(x), 2(−x); ϕ_3 = 4(x), 4(−x); ϕ_4 = x; ψ = x; rec. = x, 2(−x), x, −x, 2(x), −x. Because a selective 180° pulse for $^{13}C^{\alpha}$ in the middle of delay $2T_A$ induces a Bloch-Siegert shift to $^{13}C'$ magnetization, a careful adjustment of phase (bsp) of the last $^{13}C'$ 90°(phase y) pulse is necessary. Gradient strengths and durations: G_C = 13 k G/cm (1.6 ms), G_H = 13 k G/cm (0.4 ms). It is possible to run experiment without composite pulse ^{1}H decoupling. In that case, the low power decoupling and water selective pulses should be replaced by hard 180° pulses (marked with *asterisks*) and the relative phases of ϕ_3 and ϕ_4 should be changed by 90°. The pulse sequences code and parameter file for Varian Inova system are available from authors upon request

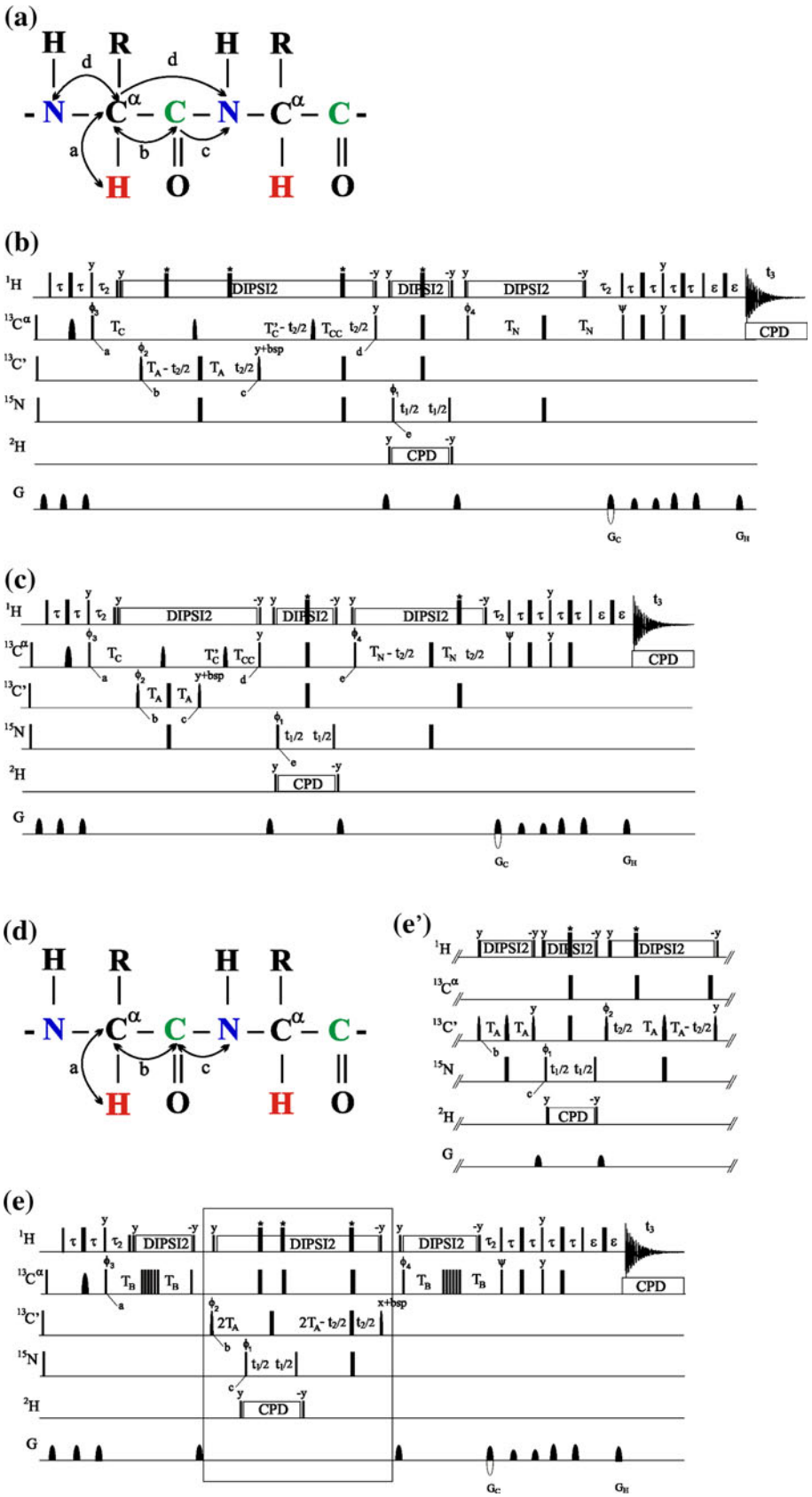
(a)
(b)
(c)
(d)
(e')
(e)
DIPSI2
CPD
t3
G
Gc
GH

$$^{1}H^{\alpha}(i) \xrightarrow{^{1}J_{HC}} {}^{13}C^{\alpha}(i) \xrightarrow{^{1}J_{C\alpha N},\,^{2}J_{C\alpha N},\,^{1}J_{C\alpha C'}} {}^{13}C'(i)$$

$$\left[T_A - t_2; {}^{1}J_{C'N}; {}^{1}J_{C\alpha N}; {}^{2}J_{C\alpha N}\right]$$

$$\xrightarrow{^{1}J_{C\alpha N},\,^{2}J_{C\alpha N},\,^{1}J_{C\alpha C'}} {}^{15}N(i)[t_1] \xrightarrow{^{1}J_{C\alpha N},\,^{2}J_{C\alpha N}} {}^{13}C^{\alpha}(i) \xrightarrow{^{1}J_{HC}} {}^{1}H^{\alpha}(i)[t_3]$$

and

$$^{1}H^{\alpha}(i) \xrightarrow{^{1}J_{HC}} {}^{13}C^{\alpha}(i) \xrightarrow{^{1}J_{C\alpha C'},\,^{1}J_{C\alpha N},\,^{2}J_{C\alpha N}} {}^{13}C'(i) - {}^{13}C^{\alpha}(i)$$

$$\xrightarrow{^{1}J_{C\alpha N},\,^{2}J_{C\alpha N},\,^{1}J_{C'N}} {}^{13}C^{\alpha}(i) \xrightarrow{^{1}J_{C\alpha C'},\,^{1}J_{C\alpha N},\,^{2}J_{C\alpha N}} {}^{15}N(i)[t_1] \xrightarrow{^{1}J_{C\alpha N},\,^{2}J_{C\alpha N}}$$

$$^{13}C^{\alpha}(i)[T_N - t_2] \xrightarrow{^{1}J_{HC}} {}^{1}H^{\alpha}(i)[t_3]$$

respectively. Active couplings employed to the magnetization transfer are indicated above the arrows and in parentheses during the constant time acquisition periods, whereas t_i ($i = 1$–3) refers to the acquisition time for the corresponding spin. Both intraresidual iH(CA)NCO and iHCAN experiments utilize a non-linearity of the N(i)-Cα(i)-C$'$(i)-N($i + 1$) spin system to obtain so-called intraresidual filtering (Permi 2002; Nietlispach et al. 2002; Jiang et al. 2005; Mäntylahti et al. 2009). Original intraresidual experiments are HN-detected out-and-back type triple-resonance experiments (Permi 2002; Nietlispach et al. 2002; Brutscher 2002; Tossavainen and Permi 2004; Nietlispach 2004) and i(HCA)CO(CA)NH is an out-and-stay type HN-detected experiment (Mäntylahti et al. 2009). Both iH(CA)NCO and iHCAN experiments presented in this work, are out-and-back type HA-detected experiments.

Both intraresidual experiments start with transfer of steady state $^{1}H^{\alpha}$ magnetization to directly bound $^{13}C^{\alpha}$ spin by using INEPT element (time point a in Fig. 1b, c; Morris and Freeman 1979). This is followed by the generation of $^{13}C^{\alpha}$-$^{13}C'$ multiple-quantum (MQ) coherence which is invoked by the 90°($^{13}C'$) pulse given at the time point b. During the ensuing t_2 period, incorporated into the delay $2T_A$, the labeling of $^{13}C'$ chemical shift takes place while $^{13}C^{\alpha}$-$^{13}C'$ magnetization becomes antiphase with respect to the adjacent $^{15}N(i + 1)$ spin at the time point c. Afterwards, the $^{13}C^{\alpha}$-$^{13}C'$ MQ coherence is converted back into the $^{13}C^{\alpha}$ single quantum (SQ) coherence, which is fully refocused at the time point d. It is noteworthy that due to rather small $^{1}J_{C\alpha N}$ and $^{2}J_{C\alpha N}$ couplings, which both evolve between time points a and d, only the pathway leading to density operator

$$\sigma(d) = N_z(i)C_z^{\alpha}(i), \tag{1}$$

immediately prior to time point d, will generate detectable magnetization at the end of the pulse sequence. Conversely, the sequential pathway, corresponding to density operator

$$\sigma(d) = C_z^{\alpha}(i)N_z(i+1), \tag{2}$$

before the time point d, is greatly suppressed (Jiang et al. 2005; Mäntylahti et al. 2009). From now on, only density operators which pass the intraresidual pathway selection and ultimately lead to observable magnetization will be considered.

The following 90°(^{15}N) pulse converts the desired coherence into the ^{15}N SQ coherence at time point e, described by the density operator

$$\sigma(e) = N_y(i)C_z^{\alpha}(i) \tag{3}$$

^{15}N chemical shift frequency is labeled during the t_1 period. Afterwards, the desired magnetization is converted back to the $^{13}C^{\alpha}$ SQ coherence and the antiphase coherence with respect to the ^{15}N(i) spin will be refocused during $2T_N$. Finally, the desired coherence will be converted back into the ^{1}H SQ coherence upon detection of $^{1}H^{\alpha}$ frequencies during t_3.

The overall transfer function $I_{\mathrm{iH(CA)NCO}}$ is proportional to

$$\begin{aligned} I_{iH(CA)NCO} \approx\ & \sin(2\pi^{1}J_{C\alpha N}(T_C + T_A))\sin(2\pi^{2}J_{C\alpha N}(T_C + T_A)) \\ & \sin^{2}(2\pi^{1}J_{C\alpha C'}T_C)\sin(2\pi^{1}J_{C'N}T_A)\cos(2\pi^{1}J_{C\alpha C\beta} \\ & (T_C + T_A + T_{CC}))\cos(2\pi^{1}J_{C\alpha C\beta}T_N)\sin(2\pi^{1}J_{C\alpha N}T_N) \\ & \cos(2\pi^{2}J_{C\alpha N}T_N)\exp(-2(T_C + T_A + T_{CC} + T_N)/T_{2,C\alpha}) \\ & \exp(-(2T_A)/T_{2,C'}), \end{aligned} \tag{4}$$

where $^{1}J_{C\alpha C'}$, $^{1}J_{C'N}$ and $^{1}J_{C\alpha C\beta}$ correspond to J coupling values of 53, 15 and 35 Hz, respectively. One-bond ($^{1}J_{C\alpha N}$) and two-bond ($^{2}J_{C\alpha N}$) couplings between backbone C$^{\alpha}$ and N are estimated to be $^{1}J_{C\alpha N} \sim 10.6$ Hz and $^{2}J_{C\alpha N}$, ~ 7.5 Hz in flexible polypeptide chain (Delaglio et al. 1991). The sensitivity of the intraresidual iHCANCO experiments is mainly governed by the transverse relaxation of $^{13}C'$ and $^{13}C^{\alpha}$ spins. Considering natively unfolded protein with relatively slow decay rates, 5 and 10 Hz, for the transverse magnetization of $^{13}C'$ and $^{13}C^{\alpha}$ spins, respectively, the optimization of delays T_A, T_C and T_{CC}, yields coherence transfer efficiency of 0.22 for iHCANCO experiments. This is comparable to the efficiency obtained for the conventional HCAN experiment (0.23). Hence, in the case of natively unfolded proteins, intraresidual HA detected experiments provide sensitivity comparable to the conventional HCAN experiment (Kay et al. 1990; Wang et al. 1995; Kanelis et al. 2000). For small globular protein (<10 kDa) with robust tertiary structure, the corresponding transfer efficiencies become less favorable to the intraresidual experiments. By assuming R_2s of 10 Hz for $^{13}C'$ and 20 Hz for $^{13}C^{\alpha}$, the transfer efficiencies for intraresidual iHCAN and conventional HCAN schemes will then become 0.077 and 0.121, respectively. This makes the exclusive intraresidual transfer less sensitive although it provides up to twofold higher resolution in comparison to the HCAN scheme. Evidently, the intraresidual transfer becomes inefficient on globular proteins larger than 10–15 kDa but it is ideally suited for the assignment of IUPs with low transfer relaxation rates.

Depending on the pulse sequence, either $^{13}C'(i)$ or $^{13}C^{\alpha}(i)$ resonance frequencies are labeled during the t_2 period. In the iH(CA)NCO scheme (Fig. 1b), the $^{13}C'(i)$ chemical shift labeling takes place during the constant-time period implemented into the $2T_A$ delay within the intraresidual filter. Therefore effective experimental resolution is restrained by the delay $(2T_C + T_{CC})$, corresponding to acquisition time of 18–22 ms in t_2 (Mäntylahti et al. 2009). However, for IUPs, chemical shift dispersion of $^{13}C'$ is often superior with respect to the frequency range found for $^{13}C^{\alpha}$ shifts as the resonance frequency of carbonyl carbon is less dependent on a residue type (Yao et al. 1997; Dyson and Wright 2001). After Fourier transformation of time domain signal in three dimensions results in cross peaks at $\omega_N(i)$, $\omega_{C'}(i)$, $\omega_{H\alpha}(i)$. Hence only single cross peak per amino acid residue, generated by the intraresidual magnetization transfer, warrants less ambiguous backbone assignment, especially on polypeptide chains with elevated motional degree of freedom. Additional virtue of intraresidual iH(CA)NCO scheme lies on differing phase properties of glycines when compared to non-glycine residues. This is due to trigonometric factors $\cos(2\pi^1J_{C\alpha C\beta}(T_C + T_A + T_{CC}))\cos(2\pi^1J_{C\alpha C\beta}T_N) \approx -1$, which is effective for non-glycine residues. The resulting 180° phase difference between glycine and non-glycine residues is especially useful for the assignment of glycines with degenerated HA shifts.

Labeling of the $^{13}C^{\alpha}$ chemical shift during the t_2 period in the iHCAN experiment (Fig. 1c) instead of the $^{13}C'$ in iH(CA)NCO, offers up to sqrt(2) times higher signal-to-noise ratio for non-glycine residues. In the case of iHCAN, the sensitivity- and gradient-enhanced coherence-order selective coherence transfer (COS-CT) can be applied during t_2 in order to transform both orthogonal $^{13}C^{\alpha}$ magnetization components simultaneously into observable ^1H SQ coherence (Kay et al. 1992; Schleucher et al. 1994). In addition, it is possible to utilize ca. 28 ms acquisition time in t_2, which offers very high resolution in the $^{13}C^{\alpha}$ dimension after mirror-image linear prediction. This technique provides an invaluable advantage when dealing with poorly dispersed cross peaks typically found in highly disordered proteins. In this case, after Fourier transform of three-dimensional time domain matrix, cross peak emerges at $\omega_N(i)$, $\omega_{C\alpha}(i)$, $\omega_{H\alpha}(i)$ i.e., again solely intraresidual correlations will be observed for each amino acid residue and that facilitates the assignment procedure.

Figure 1d schematically presents the magnetization transfer pathway used in the complementary H(CA)CON experiment, which is depicted in Fig. 1e. The experiment establishes correlation between $^1H^{\alpha}$ and $^{13}C'$ spins of the residue i and ^{15}N spin of the residue $i + 1$. The H(CA)CON experiment bears resemblance to the HCA(CO)N and H(CACO)N schemes developed by Bax and colleagues (Kay et al. 1990; Powers et al. 1991; Wang et al. 1995) as well as more recent H(CA)CON scheme (Sayers and Torchia 2001). Differences to original schemes will be briefly discussed below.

The coherence flows through the H(CA)CON experiment in the following way:

$$^1H^{\alpha}(i) \xrightarrow{^1J_{HC}} {}^{13}C^{\alpha}(i) \xrightarrow{^1J_{C\alpha C'}} {}^{13}C'(i) \xrightarrow{^1J_{C'N}} {}^{15}N(i+1)[t_1] \rightarrow$$

$$^{13}C'(i)\left[2T_A - t_2; {}^1J_{C'N}\right] \xrightarrow{^1J_{C\alpha C'}} {}^{13}C^{\alpha}(i) \xrightarrow{^1J_{HC}} {}^1H^{\alpha}(i)[t_3],$$

where active heteronuclear one-bond couplings utilized for the magnetization transfer are given above the arrows and in parentheses during the constant time acquisition periods. Different t_i $(i = 1–3)$ values refer to the acquisition time for the corresponding spin.

The experiment transfers magnetization from $^1H^{\alpha}$ to $^{13}C'$ by using consecutive INEPT steps, which utilize large one-bond couplings between $^1H^{\alpha}$ and $^{13}C^{\alpha}$ (time point a), and $^{13}C^{\alpha}$ and $^{13}C'$ (time point b), respectively. Semi-selective 180°($^{13}C^{\alpha}$) pulse could have been applied during the $^{13}C^{\alpha}$-$^{13}C'$ INEPT step in order to remove $^{13}C^{\alpha}$-$^{13}C^{\beta}$ coupling interaction during $2T_C$, but we used Shaka-6 composite pulse, which simultaneously refocuses $^{13}C^{\alpha}$ and inverts $^{13}C'$ spins for all residue types (Shaka 1985). Although semi-selective refocusing of the $^1J_{C\alpha C\beta}$ interaction drastically improves the overall sensitivity, at least by 60%, this is achieved at expense of impaired sensitivity for Ser/Gly residues, which are quite abundant in IUPs (Dyson and Wright 2005). Hence, selection of an appropriate refocusing pulse in the middle of $^{13}C^{\alpha}$-$^{13}C'$ INEPT is a trade-off between overall sensitivity and residue specificity.

A subsequent $^{13}C'$-^{15}N HMQC step is used for transferring magnetization from $^{13}C'(i)$ to the $^{15}N(i + 1)$ spin of the following residue. At time point c, $^{13}C'$-^{15}N MQ coherence is invoked by the 90°(^{15}N) pulse, which is followed by the chemical shift labeling of ^{15}N frequencies. Instead of observing the chemical shift of $^{13}C^{\alpha}$ spins during the t_2 period, the ensuing $^{13}C'$-^{15}N HMQC back-transfer is used for labeling the chemical shift of $^{13}C'$ spin of the residue i. The transfer scheme is similar to the original scheme presented by Bax and co-workers (Kay et al. 1990). However, in our case the whole $2T_A$ period is used for the chemical shift labeling of $^{13}C'$ during the $^{13}C'$-^{15}N refocusing period. This implementation enhances experimental resolution by twofold in $^{13}C'$ dimension ($t_{2,max} = 4T_A \approx$ 66 ms) when compared to the original schemes by Kay et al. (1990) and Wang and Bax (1995). In addition, to ensure high resolution in both ^{15}N and $^{13}C'$ dimensions, a number of decoupling pulses needs to applied during t_1 and t_2 periods for removal of ^{15}N-^{13}C and $^{13}C'$-$^{13}C^{\alpha}$ scalar coupling interactions during the ^{15}N and $^{13}C'$ chemical shift labeling periods. A negative aspect of using this approach stems from faster decay of ^{15}N-$^{13}C'$ MQ

coherence during the t_1 period, resulting in lower resolution along the F_1 dimension as, by assuming any cross-correlated relaxation mechanism to be negligible for ^{15}N and $^{13}C'$ spins, the linewidth in the ^{15}N dimension is determined by transverse relaxation rates of both ^{15}N and $^{13}C'$ spins.

Inset in Fig. 1e′ displays an alternative, INEPT based implementation of $^{13}C'$-^{15}N transfer and $^{13}C'$ chemical shift labeling during t_2 (Sayers and Torchia 2001). Although the resolution is limited to $t_{2,max} = 2T_A = 25–33$ ms, the experiment still offers up to fourfold to sixfold enhancement in resolution with respect to the HCA(CO)N where $t_{2,max}$ of 6–9 ms in $^{13}C^{\alpha}$ dimension can be used (Wang et al. 1995).

After labeling of $^{13}C'$ frequencies in t_2, the magnetization is transferred back to ^{1}H SQ coherence using the identical but reverse coherence transfer pathway. Finally, detection of $^{1}H^{\alpha}$ chemical shift frequencies takes place during t_3. After Fourier transformation of 3D time domain data matrix results in correlations at $\omega_N(i+1)$, $\omega_{C'}(i)$, $\omega_{H\alpha}(i)$, therefore complementing solely intraresidual correlations obtained with the iH(CA)NCO experiment.

The overall transfer function $I_{H(CA)CON}$ for the experiment is

$$I_{H(CA)CON} \approx \sin^2(2\pi J_{C\alpha C'} T_C)\sin^2(2\pi {}^1J_{C'N} T_A) \cos^2(2\pi J_{C\alpha C\beta} T_C)\exp(-4T_C/T_{2,C\alpha})\exp(-4T_A/T_{2,C'}) \quad (5)$$

Optimization of delay values using the same J coupling constants and decay rates as in the case of intraresidual experiments yields transfer efficiency of 0.28. Hence, in IUPs, the overall sensitivity of the H(CA)CON is superior to its intraresidual counterpart by $\sim 30\%$.

As mentioned above glycines are rather abundant in UIPs and therefore obtaining good quality spectrum with Gly signals is imperative. Both intraresidual and sequential HA-detected experiments utilize refocusing of the antiphase $2H_z^{\alpha}C_y^{\alpha}$ coherence to the in-phase C_x^{α} before applying coherent proton decoupling during the ^{13}C to ^{15}N magnetization transfer steps. Although this approach is superior to IS spin moieties, the glycine HA's, which establish an I_2S moiety, will be seriously deteriorated by their cross peak intensities if the refocusing and defocusing delays τ_2 are optimized for IS moieties ($\tau_2 = 1/(2\,J) = 3.4$ ms). The delay τ_2 should be a compromise between optimal values for IS and I_2S spin systems, and take into account additional signal loss for non-glycine residues due to $^{1}J_{C\alpha C\beta}$ dephasing during $2T_b$ in schemes Fig. 1e, e′. Therefore, delay τ_2 should be set to ca. 2.2–2.5 ms, which results in modest sensitivity loss, by 10–15%, for non-glycine residues but enables clear detection of glycines. Alternative implementation for decoupling of $^{1}J_{HX}$ (where X is either ^{13}C or ^{15}N) interaction during the courses of intraresidual and sequential experiments is also shown in Fig. 1b, c, e, e′. The antiphase $2H_z^{\alpha}C_y^{\alpha}$ coherence is not rephased and composite pulse decoupling is replaced by several 180° proton pulses (denoted by asterisks in Fig. 1) during the experiments. There is no sensitivity loss associated with incomplete rephasing and dephasing of the antiphase and in-phase coherences during delays τ_2. However, we observed significant loss in sensitivity for methine moieties in GB1 due to contribution of ^{1}H-^{1}H spin flips to relaxation rates of ^{13}C and ^{15}N coherences. Hence, we prefer utilizing composite pulse decoupling for removal of $^{1}J_{HX}$ interaction during the experiments.

The final advantage of the new experiment regards water suppression. Although sensitivity enhanced gradient selected echo/antiecho coherence transfer is superfluous in the intraresidual iH(CA)NCO and sequential H(CA)CON experiments, both schemes utilize the gradient echo together with the water flip-back approach for efficient water suppression, enabling measurements to be carried out in $^{1}H_2O$. Water flip-back is obtained by refocusing the antiphase $2H_z^{\alpha}C_y^{\alpha}$ magnetization during the τ_2 delay to C_x^{α} and subsequently applying two semi-selective pulses to water frequency. In this way, water magnetization will be spin-locked along the x-axis during the proton decoupling and will be returned back to positive z-axis prior to acquisition.

Sometimes it may be advantegous to dissolve protein in $^{2}H_2O$, especially if protein stability requires use of alkali pH. To that end, additional ^{2}H decoupling during ^{15}N (t_1) evolution should be utilized for removal of J-coupling between ^{15}N and ^{2}H. However, in case of highly mobile IUPs this does not provide significant advantage due to very short longitudinal relaxation time of ^{2}H spins.

Application to GB1 and natively unfolded $EspF_U$ R47

We applied the proposed pulse sequences for two proteins, a 56-residue immunoglobulin-binding domain B1 of streptococcal protein G (GB1, 6.5 kDa), and fifth repeat of enterohemorrhagic *Escherichia coli* effector ($EspF_U$). GB1 is small and very stable globular protein, which has been extensively studied by NMR spectroscopy, whereas EspFu is reported to bind GTPase binding domain (GBD) in Wiskott-Aldrich syndrome protein (WASP) family (Cheng et al. 2008). The fifth repeat of $EspF_U$ comprises 47 residues from which 10 residues are prolines. $EspF_U$ exhibits a collapsed chemical shift dispersion and low ^{15}N heteronuclear NOEs, which can be attributed to natively unfolded protein. Therefore GB1 and $EspF_U$ establish a good benchmark for the HA-based assignment strategy for disordered proteins.

Resolution enhancement in the $^{13}C'$ dimension, obtained by employing the HMQC-like $^{13}C'$-^{15}N transfer in the H(CA)CON experiment, can be easily observed by comparing two-dimensional $^{13}C'$-$^{1}H^{\alpha}$ correlation spectra in Fig. 2a, b, recorded with the H(CA)CON schemes of

Fig. 1e, e′, respectively. Figure 2c displays overlaid two-dimensional ^{15}N-^{1}H$^{\alpha}$ correlation maps of GB1, recorded as 2D versions of the three-dimensional intraresidual iHCAN (black contours) and H(CA)CON (red contours) experiments. For the purpose of proof of principle, sequential walk has been traced out for residues A25-V31, where intraresidual ^{15}N(i)-^{1}H$^{\alpha}$(i) connectivities are indicated with their corresponding residue numbers. Even though GB1 is a very rigid globular protein and almost completely lacking disordered regions, there is still a significant resonance overlap existing in the ^{15}N-^{1}H$^{\alpha}$ map. For instance, ^{15}N frequencies, and hence intraresidual and sequential correlations, are almost completely overlapping for E29-K30 and V31-F32 residue pairs. Notable is the efficient water suppression obtained with combined use of water flip-back and heteronuclear gradient echo, which enabled high-quality data collection in $^{1}H_2O$ sample at 800 ^{1}H MHz. We also compared the sensitivities between the iH(CA)N(CO) and HCAN experiments. Relative sensitivities of the attainable *intraresidual* correlations in GB1 for iH(CA)N(CO) were 10 ± 10% weaker than in the corresponding resonances in the HCAN spectrum, which is good accordance with theoretical calculations for small globular protein (vide supra). Two-dimensional ^{15}N-^{1}H$^{\alpha}$ planes for the intraresidual iH(CA)N(CO) and conventional HCAN experiments are shown in Supplementary Fig. 1.

Assignment of natively unfolded proteins is significantly more challenging in terms of resonance overlap. We

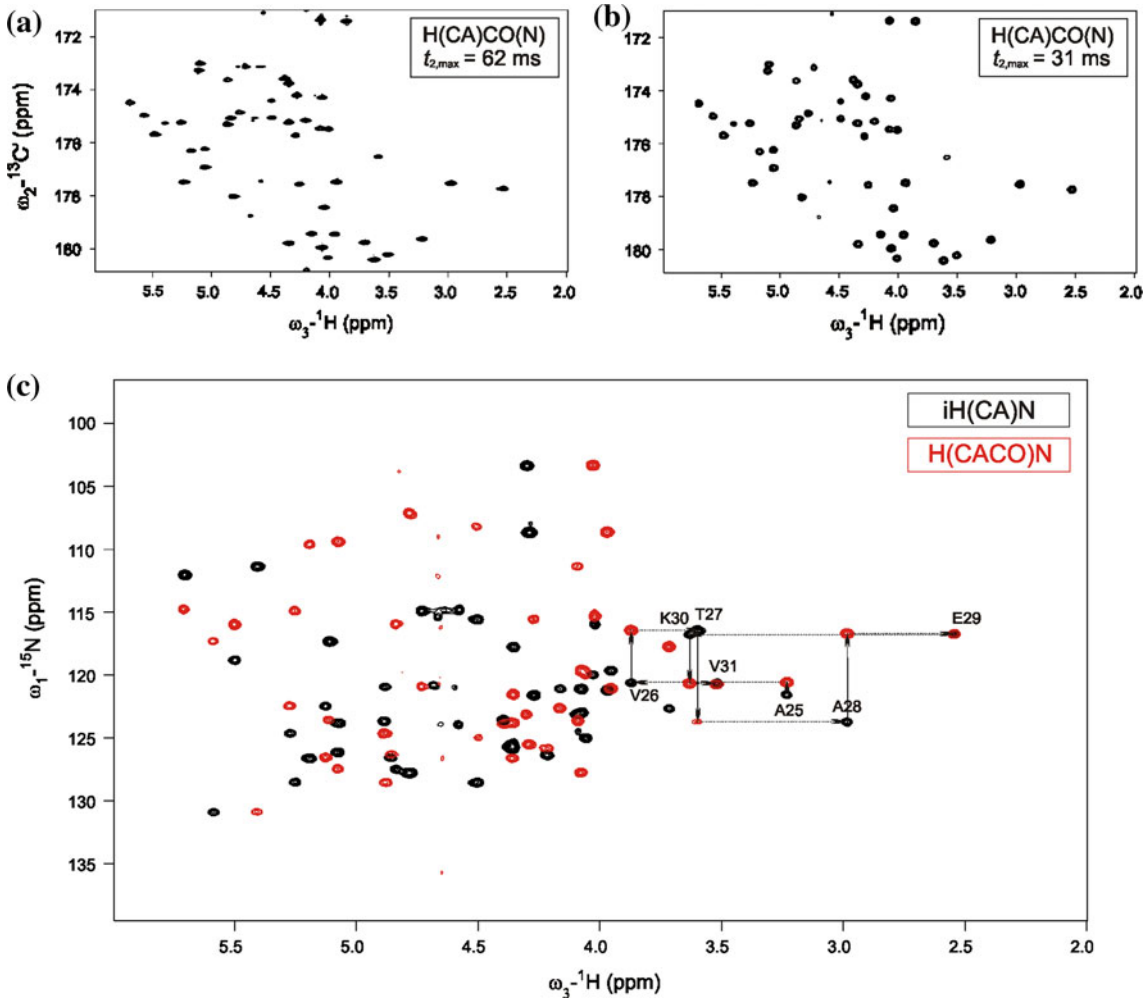

Fig. 2 Two-dimensional ^{13}C′(i)-^{1}H$^{\alpha}$(i) correlation plots of ^{13}C/^{15}N labeled GB1, recorded with **a** H(CA)CON scheme with the ^{13}C′-^{15}N HMQC transfer (Fig. 1e) and **b** H(CA)CON scheme with the ^{13}C′-^{15}N INEPT transfer (Fig. 1e′). **c** Two-dimensional ^{15}N(i)-^{1}H$^{\alpha}$(i) and ^{15}N(i + 1)-^{1}H$^{\alpha}$(i) correlation plots of ^{13}C/^{15}N labeled GB1, acquired with three-dimensional iHCAN (Fig. 1c) and H(CA)CON (Fig. 1e) experiments without t_2 (^{13}C) incrementation. Intraresidual spectrum, showing ^{15}N(i)-^{1}H$^{\alpha}$(i) correlations (*black contours*), and sequential spectrum exhibiting ^{15}N(i + 1)-^{1}H$^{\alpha}$(i) correlations (*red contours*) are superimposed. Sequential assignment has been traced out for polypeptide stretch from A35 to V31, and the corresponding residues are marked with appropriate numbers on intraresidual connectivities. Spectra were processed using identical weighting functions and data matrix sizes and are shown with identical contour levels, using a spacing factor of 1.2

applied intraresidual iH(CA)NCO and iHCAN experiments (Fig. 1b, c) together with their complementary H(CA)CON (Fig. 1e) and HCA(CO)N (Wang et al. 1995) counterparts for the assignment of uniformly labeled $^{15}N/^{13}C$ $EspF_U$. Figure 3 shows $^{1}H(i)$-$^{13}C'(i)$ (panel a) and $^{1}H(i)$-$^{13}C^{\alpha}(i)$ (panel b) projections of the three-dimensional iH(CA)NCO and iHCAN spectra, respectively. The corresponding $^{13}C'(i)$-$^{15}N(i)$ and $^{13}C^{\alpha}(i)$-$^{15}N(i)$ projections are shown in panels c and d, respectively. As expected, the dispersion of cross peaks in $^{13}C'(i)$-$^{15}N(i)$ plane is slightly larger in comparison to the $^{13}C^{\alpha}(i)$-$^{15}N(i)$ map owing to more favorable frequency distribution of $^{13}C'(i)$ chemical shifts. On the other hand, this is counterbalanced by a higher resolution obtained in the $^{13}C^{\alpha}(i)$ dimension. Representative $^{15}N(i)$-$^{1}H^{\alpha}(i)$ (e and g) and $^{15}N(i+1)$-$^{1}H^{\alpha}(i)$ (f and h) strip plots are extracted from the $^{13}C'(i)$ (left panel) or $^{13}C^{\alpha}(i)$ (right panel) chemical shift of P31-A35 residues. As can be appreciated from strips P31 and P34, prolines have a characteristic downfield chemical shift with respect to majority of residues which facilitates the assignment procedure. In accordance with our presumption, the use of $^{13}C'$ instead of $^{13}C^{\alpha}$ chemical shift for the assignment offers less crowded strips due to smaller dependence of $^{13}C'$ chemical shift on residue type. This makes assignment more straightforward with respect to the $^{13}C^{\alpha}$ based approach. Using this procedure, we were able to obtain complete assignment of $^{1}H^{\alpha}$, $^{13}C^{\alpha}$, $^{13}C'$ and ^{15}N nuclei despite the very poorly dispersed ^{15}N-HSQC spectrum, a few Pro-Pro dipeptide stretches and the presence of multiple conformations stemming from prolines populating both *cis* and *trans* isomers. Very long flexible polypeptides may require additional resolution to minimize cross peak overlap. To that end, four-dimensional iHCANCO and HCACON experiments correlating $^{1}H^{\alpha}(i)$, $^{13}C^{\alpha}(i)$, $^{13}C'(i)$, $^{15}N(i)$ and $^{1}H^{\alpha}(i)$, $^{13}C^{\alpha}(i)$, $^{13}C'(i)$, $^{15}N(i+1)$ nuclei may be highly useful. In order to keep experimental time reasonable, it is possible to utilize recently introduced non-uniform or radial sampling schemes for recording high-resolution 4D data sets (Barna et al. 1987; Freeman and Kupce 2004; Rovnyak et al. 2004; Marion 2006; Kazimierczuk et al. 2006; Coggins and Zhou 2008; Jaravine et al. 2008).

Conclusions

In this work, we have introduced new protocol for the sequential assignment of natively unfolded proteins. The proposed protocol relies on a few key advantages. HA detection enables: (i) assignment of natively unfolded proteins at any pH i.e., it is not sensitive to rapid chemical exchange ongoing in natively unfolded proteins even at moderately high pH, (ii) straightforward assignment of proline-rich polypeptides without additional proline-customized experiments, and (iii) more streamlined and less ambiguous assignment based on solely intraresidual $^{15}N(i)$-$^{13}C'(i)$-$H^{z}(i)$ and sequential $^{15}N(i+1)$-$^{13}C'(i)$-$H^{z}(i)$ magnetization transfer together with use of less residue dependent chemical shifts of ^{15}N and $^{13}C'$ nuclei. We have applied this assignment approach to the fifth repeat of $EspF_U$, which is natively unfolded, proline-rich sequence, containing 47 residues. Using the proposed experiments, we were able to assign 90% of $^{1}H^{\alpha}$, $^{13}C^{\alpha}$, $^{13}C'$, ^{15}N chemical shifts in $EspF_U$. Theoretical analysis and experimental results shown in this work suggest that the introduced approach and pulse sequences will be useful in the assignment of natively unfolded proline-rich proteins or polypeptide chains.

Materials and methods

Both intraresidual iH(CA)NCO and iHCAN experiments as well as sequential H(CA)CON, and HCA(CO)N (Wang et al. 1995) experiments were applied to experimental verification on two proteins: 1.5 mM uniformly $^{15}N/^{13}C$ labeled immunoglobulin-binding domain B1 of streptococcal protein G (GB1, 6.5 kDa, 56 residues) dissolved in 20 mM potassium phosphate buffer, pH 5.5 with 7% D_2O in a 250 µl Shigemi micro-cell, and 1 mM uniformly $^{15}N/^{13}C$ labeled fifth repeat of enterohemorrhagic *Escherichia coli* effector ($EspF_U$, with 47 residues), dissolved in buffer containing 20 mM sodium phosphate pH 7.0 and 50 mM NaCl, supplemented with 7% D_2O in a 250 µl Shigemi micro-cell.

All the spectra were recorded at 25°C, on a Varian Unity INOVA 800 NMR spectrometer, equipped with a $^{15}N/^{13}C/^{1}H$ triple-resonance probehead and an actively shielded *Z*-axis gradient system. Two-dimensional H(CA)CO(N) spectra (Fig. 2a, b), measured with the pulse sequences shown in Fig. 1e (and Fig. 1e′), were recorded using 8 (16) transients per FID with 124 (62) and 1,024 complex points, corresponding to acquisition times of 62 (31) and 64 ms in t_2 (^{13}C) and t_3 (^{1}H). Two-dimensional iH(CA)N spectrum of GB1 shown in Fig. 2c, was recorded using 32 transients per FID with 96 and 1,024 complex points, corresponding to acquisition times of 27 and 64 ms in t_1 (^{15}N) and t_3 (^{1}H). The total experimental time was 2 h. The corresponding two-dimensional H(CACO)N spectrum was recorded with identical parameters except for 8 transients, resulting in total experimental time of 30 min. Intraresidual iH(CA)NCO (and iHCAN) spectra of $EspF_U$ R47 were recorded with 4 (2) transients per FID using 96, 36 (150) and 1,024 complex points in ^{15}N, $^{13}C'(^{13}C^{\alpha})$ and ^{1}H dimensions. This corresponds to acquisition times of 27, 18 (25) and 64 ms in t_1, t_2 and t_3, respectively. The complementary H(CA)CON (and HCA(CO)N) spectra were recorded with four transients per FID using 96, 36 (41) and

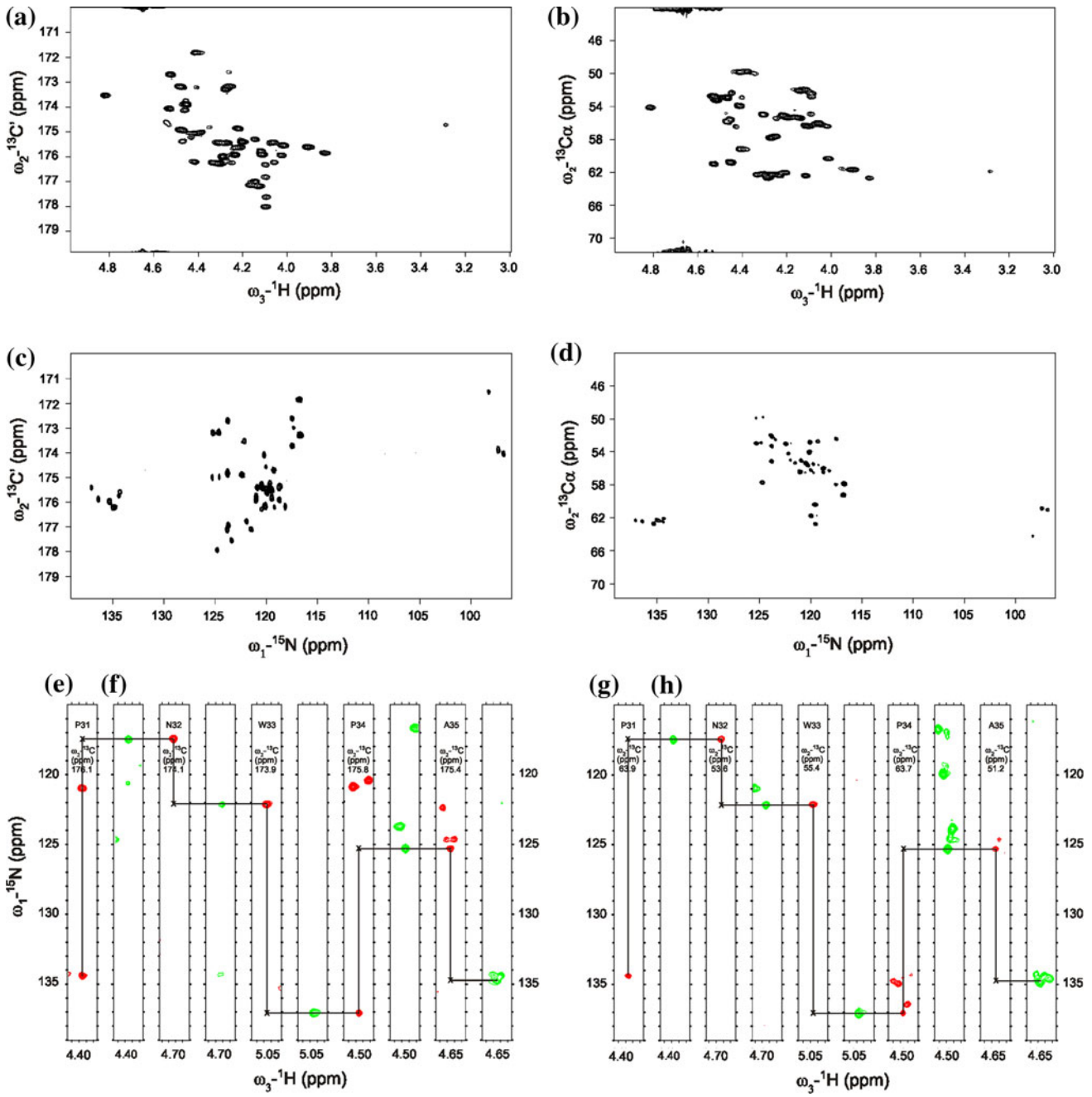

Fig. 3 $^{1}H(i)$-$^{13}C'(i)$ (*panel a*), $^{1}H(i)$-$^{13}C^{\alpha}(i)$ (*panel b*), $^{15}N(i)$-$^{13}C'(i)$, (*panel c*) and $^{15}N(i)$-$^{13}C^{\alpha}(i)$ (*panel d*) projections from three-dimensional iH(CA)NCO and iHCAN spectra, recorded with pulse sequences shown in **b** and **c**, respectively. $^{15}N(i)$-$^{1}H^{\alpha}(i)$ (**e**, **g**) and $^{15}N(i+1)$-$^{1}H^{\alpha}(i)$ (**f**, **h**) strip plots are taken at the chemical shift of $^{13}C'(i)$ (*panels e* and *f*) and $^{13}C^{\alpha}(i)$ (*panels g* and *h*). 'Sequential walk' by employing iH(CA)NCO/H(CA)CON and iHCAN/HCA(CO)N experiments is shown for the assignment of residues P31-A35 of $R47_5$. *Black crosses* indicate positions of the suppressed correlations originating from the sequential pathway

1,024 complex points in ^{15}N, $^{13}C'$ ($^{13}C^{\alpha}$) and ^{1}H dimensions, which is equal to acquisition times of 27, 18 (6.8) and 64 ms in t_1, t_2 and t_3, respectively.

Spectra were processed using the standard VNMRJ 2.1 revision B software package (Varian Inc., 2006) and analyzed with VNMRJ 2.1 revision B and Sparky 3.1.10 (Goddard and Kneller 2004). Prior to zero-filling to two-dimensional 1,024 × 4,096 data matrix (Fig. 2), or three-dimensional 512 × 512 × 2,048 data matrix (Fig. 3a–h) followed by the Fourier transform, the data were weighted with a shifted squared sine–bell functions applied to all three dimensions.

Acknowledgments This work was financially supported by the grants 122170 and 131144 (to P. P.) from the Academy of Finland. We thank Vytautas Raulinaitis for useful discussions, and Elina Ahovuo and Jessica Buchmüller for excellent technical assistance.

References

Alho N, Klaavuniemi T, Ylanne J, Permi P, Mattila S (2007) Backbone NMR assignment of the internal interaction site of ALP. Biomol NMR Assign 1:85–87

Bai Y, Milne JS, Mayne L, Englander SW (1993) Primary structure effects on peptide group hydrogen exchange. Proteins Struct Funct Genet 17:75–86

Barna JCJ, Laue ED, Mayger MR, Skilling J, Worrall SJP (1987) Exponential sampling, an alternative method for sampling in two-dimensional NMR experiments. J Magn Reson 73:69–77

Bendall MR (1995) Heteronuclear J coupling precession during spin-lock and adiabatic pulses. Use of adiabatic inversion pulses in high-resolution NMR. J Magn Reson A116:46–58

Bermel W, Bertini I, Felli IC, Piccioli M, Pierattelli R (2006) ^{13}C-detected protonless NMR spectroscopy of proteins in solution. Prog Nucl Magn Reson Spectr 48:25–45

Bermel W, Bertini I, Csizmok V, Felli IC, Pierattelli R, Tompa P (2009) H-start for exclusively heteronuclear NMR spectroscopy: the case of intrinsically disordered protein. J Magn Reson 198:275–281

Bottomley MJ, Macias MJ, Liu Z, Sattler M (1999) A novel NMR experiment for the sequential assignment of proline residues and proline stretches in ^{13}C/^{15}N-labeled proteins. J Biomol NMR 13:381–385

Brutscher B (2002) Intraresidue HNCA and COHNCA experiments for protein backbone resonance assignment. J Magn Reson 156:155–159

Cheng HC, Skehan BM, Campellone KG, Leong JM, Rosen MK (2008) Structural mechanism of WASP activation by the enterohaemorrhagic *E. coli* effector EspF(U). Nature 454: 1009–1013

Coggins BE, Zhou P (2008) High resolution 4-D spectroscopy with sparse concentric shell sampling and FFT-CLEAN. J Biomol NMR 42:225–239

Delaglio F, Torchia DA, Bax A (1991) Measurement of ^{15}N–^{13}C J couplings in staphylococcal nuclease. J Biomol NMR 1:439–446

Dyson HJ, Wright PE (2001) Nuclear magnetic resonance methods for elucidation of structure and dynamics in disordered states. Methods Enzymol 339:258–270

Dyson HJ, Wright PE (2005) Intrinsically unstructured proteins and their functions. Nat Rev Mol Cell Biol 6:197–208

Freeman R, Kupče E (2004) Distant echoes of the accordion: reduced dimensionality, GFT-NMR, and projection-reconstruction of multidimensional spectra. Concepts Magn Reson 23A:63–75

Goddard TD, Kneller DG (2004) SPARKY 3. University of California, San Francisco

Grzesiek S, Bax A, Hu J-S, Kaufman J, Palmer I, Stahl SJ, Tjandra N, Wingfield PT (1997) Refined solution structure and backbone dynamics of HIV-1 Nef. Prot Sci 6:1248–1263

Hu K, Vögeli B, Clore GM (2007) Spin-state selective carbon-detected HNCO with TROSY optimization in all dimensions and double echo-antiecho sensitivity enhancement in both indirect dimensions. J Am Chem Soc 129:5484–5491

Jaravine VA, Zhuravleva AV, Permi P, Ibraghimov I, Orekhov VY (2008) Hyperdimensional NMR spectroscopy with nonlinear sampling. J Am Chem Soc 130:3927–3936

Jiang L, Coggins BE, Zhou P (2005) Rapid assignment of protein side chain resonances using projection-reconstruction of (4, 3)D HC(CCO)NH and intra-HC(C)NH experiments. J Magn Reson 175:170–176

Kanelis V, Donaldson L, Muhandiram DR, Rotin D, Forman-Kay JD, Kay LE (2000) Sequential assignment of proline-rich regions in proteins: application to modular binding domain complexes. J Biomol NMR 16:253–259

Kay LE, Ikura M, Tschudin R, Bax A (1990) Three-dimensional triple-resonance NMR spectroscopy of isotopically enriched proteins. J Magn Reson 89:496–514

Kay LE, Keifer P, Saarinen T (1992) Pure absorption gradient enhanced heteronuclear single quantum correlation spectroscopy with improved sensitivity. J Am Chem Soc 114:10663–10665

Kazimierczuk K, Zawadzka A, Koźmiński V, Zhukov I (2006) Random sampling of evolution time space and Fourier transform processing. J Biomol NMR 36:157–168

Kupće E, Wagner G (1995) Wideband homonuclear decoupling in protein spectra. J Magn Reson 109A:329–333

Mäntylahti S, Tossavainen H, Hellman M, Permi P (2009) An intraresidual i(HCA)CO(CA)NH experiment for the assignment of main-chain resonances in 15N, 13C labeled proteins. J Biomol NMR 45:301–310

Marion D (2006) Processing of ND NMR spectra sampled in polar coordinates: a simple Fourier transform instead of a reconstruction. J Biomol NMR 36:45–54

Marion D, Ikura M, Tschudin R, Bax A (1989) Rapid recording of 2D NMR-spectra without phase cycling–application to the study of hydrogen-exchange in proteins. J Magn Reson 85:393–399

Morris GA, Freeman R (1979) Enhancement of nuclear magnetic resonance signals by polarization transfer. J Am Chem Soc 101:760–762

Nietlispach D (2004) A selective intra-HN(CA)CO experiment for the backbone assignment of deuterated proteins. J Biomol NMR 28:131–136

Nietlispach D, Ito Y, Laue ED (2002) A novel approach for the sequential backbone assignment of larger proteins: selective intra-HNCA and DQ-HNCA. J Am Chem Soc 124:11199–11207

Permi P (2002) Intraresidual HNCA: an experiment for correlating only intraresidual backbone resonances. J Biomol NMR 23:201–209

Permi P, Annila A (2004) Coherence transfer in proteins. Prog Nucl Magn Reson Spectr 44:97–137

Pervushin K, Riek R, Wider G, Wüthrich K (1997) Attenuated T2 relaxation by mutual cancellation of dipole-dipole coupling and chemical shift anisotropy indicates an avenue to NMR structures of very large biological macromolecules in solution. Proc Natl Acad Sci U S A 94:12366–12731

Powers R, Gronenborn AM, Clore GM, Bax A (1991) Three-dimensional triple-resonance NMR of ^{13}C/^{15}N-enriched proteins using constant-time evolution. J Magn Reson 94:209–213

Rovnyak D, Frueh DP, Sastry M, Sun Z-YJ, Stern AS, Hoch JC, Wagner G (2004) Accelerated acquisition of high resolution triple-resonance spectra using non-uniform sampling and maximum entropy reconstruction. J Magn Reson 170:15–21

Sattler M, Schleucher J, Griesinger C (1999) Heteronuclear multidimensional NMR experiments for the structure determination of proteins in solution employing pulsed field gradients. Prog Nucl Magn Reson Spectr 34:93–158

Sayers EW, Torchia DA (2001) Use of the carbonyl chemical shift to relieve degeneracies in triple-resonance assignment experiments. J Magn Reson 153:246–253

Schleucher J, Schwendinger MG, Sattler M, Schmidt P, Glaser SJ, Sørensen OW, Griesinger C (1994) A general enhancement scheme in heteronuclear multidimensional NMR employing pulsed-field gradients. J Biomol NMR 4:301–306

Shaka AJ (1985) Composite pulses for ultra-broadband spin inversion. Chem Phys Lett 120:201–205

Shaka AJ, Keeler J, Frenkiel T, Freeman R (1983) An improved sequence for broad-band decoupling–Waltz-16. J Magn Reson 52:335–338

Silver MS, Joseph RJ, Hoult DI (1984) Highly selective $\pi/2$ and π pulse generation. J Magn Reson 59:347–351

Tompa P (2002) Intrinsically unstructured proteins. Trends Biochem Sci 27:527–533

Tossavainen H, Permi P (2004) Optimized pathway selection in intraresidual triple-resonance experiments. J Magn Reson 170:244–251

Varian Inc. NMR Systems (2006) Varian NMR Systems with VNMRJ Software

Wang AC, Bax A (1995) Reparametrization of the Karplus relation for $^{3}J(H^{\alpha}–N)$ and $^{3}J(H^{N}–C')$ in peptides from uniformly $^{13}C/^{15}N$-enriched human ubiquitin. J Am Chem Soc 117:1810–1813

Wang A, Grzesiek S, Tschudin R, Lodi PJ, Bax A (1995) Sequential backbone assignment of isotopically enriched proteins in D_20 by deuterium-decoupled HA(CA)N and HA(CACO)N. J Biomol NMR 5:376–382

Yamazaki T, Lee W, Arrowsmith CH, Muhandiram DR, Kay LE (1994) A suite of triple-resonance NMR experiments for the backbone assignment of ^{15}N, ^{13}C, ^{2}H labeled proteins with high-sensitivity. J Am Chem Soc 116:11655–11666

Yao J, Dyson HJ, Wright PE (1997) Chemical shift dispersion and secondary structure prediction in unfolded and partly folded proteins. FEBS Lett 419:285–289